Chemical Physics 556 (2022) 111470

Contents lists available at ScienceDirect

Chemical Physics

journal homepage: www.elsevier.com/locate/chemphys

Spodium and tetrel bonds involving Zn(II)/Cd(II) and their interplay

Na Liu [a], Qingzhong Li [a,*], Steve Scheiner [b,*]

[a] The Laboratory of Theoretical and Computational Chemistry, School of Chemistry and Chemical Engineering, Yantai University, Yantai 264005, PR China
[b] Department of Chemistry and Biochemistry, Utah State University, Logan, UT 84322-0300, USA

ARTICLE INFO

Keywords:
Cooperativity
Synergy
Noncovalent bond
Molecular electrostatic potential

ABSTRACT

Ab initio calculations consider $SpCO_3/SpSO_4/SpCl_2$ (Sp = Zn(II), Cd(II)) as molecules that can engage in both a spodium bond or a tetrel bond through O or Cl. NCH, $NHCH_2$, and NH_3 are considered as Lewis bases. The Sp···N spodium bonds are very strong, with interaction energies in the 12–59 kcal/mol range. Those bonds involving Zn are somewhat stronger than Cd, and bond strength diminishes in the $SO_4 > CO_3 \gg 2Cl$ ligand order. Tetrel bonds between the Si of SiH_3F and a O or Cl atom of the ligand are of moderate strength of 2–9 kcal/mol. In triads in which both a spodium and tetrel bond are simultaneously present, there is a positive cooperativity between them. The bond enhancement is particularly significant in the tetrel bond, whose strength can reach as much as 15 kcal/mol within the trimer.

1. Introduction

The interactions between different types of molecules are very important in the fields of chemistry, biology, and physics [1–3], which has motivated years of progress in related research. Like the H-bond, the closely related halogen bond has applications in crystal materials [4–6], chemical reactions [7], molecular self-assembly [8], molecular recognition [9] and other aspects [10]. A concept that has found wide application, and which is a feature common to many, is the σ-hole, a region of positive electrostatic potential on a formally electronegative atom, along the extension of a covalent bond [11–13]. This positive area is able to attract the negative region of a nucleophile, and set off a cascade of other forces including charge transfer and dispersion.

Adding to the already growing list of noncovalent bonds, including the halogen and chalcogen bonds, Bauzá et al. recently proposed the idea of a Sp···X "spodium bond" [14] based on their studies of SpX_2L_2 where Sp refers to the 12th Group elements Zn, Cd, or Hg. The earliest description of an interaction of this type arose from the structure of dichlorobis (thiosemicarbazide)mercury(II) [15], with its infinite one-dimensional supramolecular chain. The distance between the electron donor (chlorinated ligand) and the Hg-Cl bond is 3.25 Å, which is slightly shorter than the sum of van der Waals radii (3.30 Å) and significantly longer than the sum of covalent radii (2.39 Å). Frenking et al [16] studied the geometric and energetic characteristics of carbonyl complexes $[Sp(CO)_n]^{2+}$ and found that the Sp···C—O bond strength diminished in the order $Zn^{2+} > Hg^{2+} > Cd^{2+}$. SpX_2 (Sp = Zn, Cd; X = Cl, Br) forms a stable π-complex with neutral diborenes with a high-lying π(B=B) orbital [17]. The spodium bond concept also applies to intramolecular interactions [18,19].

In a parallel line, the manner in which the 14th Group elements C, Si, Ge etc engage in similar sorts of noncovalent bonds has been the object of a good deal of study in recent years [20–25]. One of the first identifications of this so-called tetrel bond [26] was made in 2009 [21], and was used to explain why the bond angle of SiO•••N is reduced in the order $FH_2SiONMe_2 > F_3SiONMe_2 > H_3SiONMe_2$ [27]. Among the chief features of the tetrel bond is the growth in its strength connected with a heavier tetrel atom, which is associated with a deeper σ-hole [28]. As the lightest in this group, carbon seldom participates in tetrel bonds unless it is adjoined with strong electron-withdrawing substituents or a strong base acts as a nucleophile. For example, the C atom in CH_4 does not engage in such bonds, whereas CH_3OH and CH_3F can do so [29]. In addition to the sensitivity of the tetrel bond strength to the identify of the tetrel atom and its accompanying σ-hole [30], the nucleophilicity of the partner base plays a key role as well. The most common electron donor bases are lone pair electrons [31], π-electrons [32], metal hydrides [33,34], radicals [35] and carbenes [36,37]. Because of the heavy preponderance of alkyl groups in proteins and other biological systems, elucidation of the properties of the tetrel bond will be crucial to a full understanding of their structure and function [29].

One of the more intriguing aspects of the tetrel bond, and others in that family, is their cooperativity with one another. Synergy can occur when the tetrel bond is combined with hydrogen bonds [38], lithium

* Corresponding authors.
E-mail addresses: lqz@ytu.edu.cn (Q. Li), steve.scheiner@usu.edu (S. Scheiner).

https://doi.org/10.1016/j.chemphys.2022.111470
Received 11 January 2022; Received in revised form 29 January 2022; Accepted 30 January 2022
Available online 4 February 2022

bonds [39], chalcogen bonds [40], or with itself [41]. For example, in F_2TO-NCH-NCH (T = C and Si), the tetrel and hydrogen bonds reinforce one another, while the two TBs show negative synergy [38] in HCN-FT_2O-NCH. Esrafili et al. studied the cooperative effect in YH_3T-NCX-NH_3 (Y = F, CN; T = C, Si; X = Cl, SH, PH_2), where a tetrel bond coexists with a halogen bond, chalcogen bond, or pnictogen bond [42]. This synergistic effect is of great importance in the fields of crystal materials, chemical reactions, and molecular recognition [43–45]. For example, the self-assembly of molecules on a surface can be regulated by synergistic effects [46].

The first objective of the current study is an extension of our tentative understanding of the spodium bond. This interaction is quite new and has undergone only limited study to date. The Group 12 atoms Sp = Zn and Cd are integrated into a molecule that contains CO_3 and SO_4 as ligands, wherein Sp is ditopically attached to two of the O atoms of the ligand. So as to consider whether this dipodal bonding has a perturbing effect, Sp was also liganded by a pair of separate Cl atoms. Altogether, these $SpCO_3$, $SpSO_4$, and $SpCl_2$ (Sp = Zn(II), Cd(II)) units comprise an overall neutral Lewis acid. As another consideration, these molecules are also important inorganic materials in their own right. So as to systematically consider a range of base strength, these molecules are paired with each of N≡CH, NH=CH_2, and NH_3. As seen below, this coordination makes the resulting spodium bond very strong indeed, even rivalling covalent bonds, and the calculations analyze the source of this unexpected strength. With regard to a tetrel bond, the O or Cl atoms of the $SpCO_3$, $SpSO_4$, and $SpCl_2$ units were allowed to interact with the Si atom of SiH_3F. Any synergy between the ensuing spodium and tetrel bonds is examined in the context of the triad where both of these bonds are present. All told, the calculations described below compare 18 different spodium-bonded dimers, 6 dyads containing a tetrel bond, and 16 triads in which both sorts of bonds are present simultaneously.

2. Theoretical methods

Second-order Møller–Plesset perturbation theory (MP2) was used to incorporate electron correlation in conjunction with the aug-cc-pVTZ basis set. For the Zn and Cd atoms, the aug-cc-pVTZ-PP basis set including a pseudo-potential was adopted to account for relativistic effects [47]. The similar consideration has been made for other metal complexes [48–53]. The geometries of all species were fully optimized, and ensuing frequency calculations confirmed them as true minima. The interaction energy was defined as the difference between the energy of each complex and the monomer sum with their geometries taken from that adopted within the complex. This quantity was corrected for basis set superposition error (BSSE) by the counterpoise procedure advocated by Boys and Bernardi [54]. All calculations were performed using the Gaussian 09 package of codes [55].

The molecular electrostatic potentials (MEPs) of monomers and complexes on the 0.001e $Bohr^{-3}$ isosurface were calculated by using the wave Function Analysis-Surface Analysis Suite (WFA-SAS) program [56]. Atoms in molecules (AIM) analysis was performed to obtain topological parameters of each bond critical point (BCP), including electron density (ρ), its Laplacian ($\nabla^2\rho$) and total energy density (H) via QTAIM software [57]. Natural bond orbital (NBO) analysis implemented by the NBO 6.0 program [58] provided information concerning charge transfer and its energetic implications. Multiwfn and VMD [59,60] were utilized to map noncovalent interactions (NCI) [61]. Energy decomposition calculations were carried out by the localized molecular orbital-energy decomposition analysis (LMO-EDA) method [62] using the GAMESS program [63].

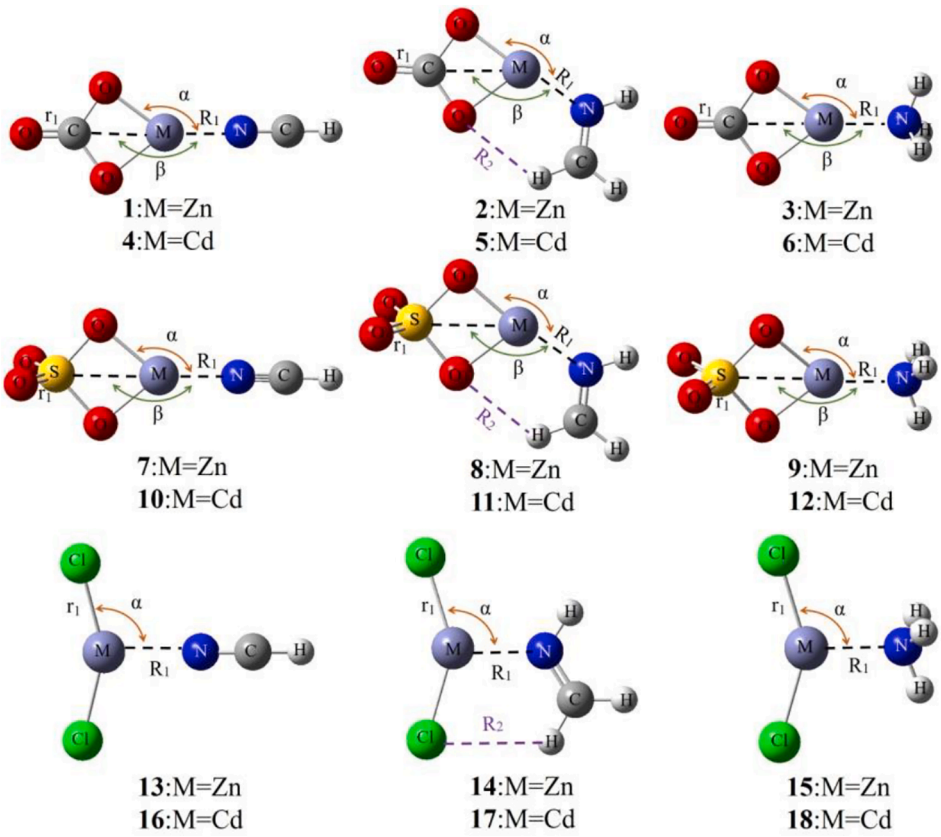

Fig. 1. Optimized geometries of spodium-bonded binary complexes.

3. Results

3.1. Spodium-bonded binary complexes

The geometries of the spodium-bonded dyads are illustrated in Fig. 1, along with definitions of the important geometrical parameters. Whether Zn or Cd, the metal atom Sp is symmetrically disposed between the two O atoms of CO_3^{2-} or SO_4^{2-}, and likewise for the two Cl substituents in $SpCl_2$. The overall charge of each of the three Lewis acids is zero. The metal atom interacts with the N atom of the NCH, $NHCH_2$, and NH_3 bases that place the N atom in sp, sp^2, and sp^3 hybridization, respectively. The R(Sp···N) intermolecular distance is defined as R_1; R_2 refers to the fairly close distance between a methylene H atom of $NHCH_2$ and the O or Cl atom of the acid, and may in principle refer to a H-bond length (see below). The α angle locates the base N atom with respect to one of the two O/Cl atoms of the acid substituent. β refers to the OCO bisector of CO_3^{2-} and the OSO bisector of SO_4^{2-}, as delineated in Fig. 1.

Table 1 collects the relevant geometric parameters for all 18 of the dyads. The intermolecular R_1 distance is shorter for Zn than for the larger Cd atom, as one might expect. In most cases, this distance is shorter for the $NHCH_2$ base than for NCH and NH_3, which may be due to the secondary CH···O/Cl H-bond which is apparently present. Note for example, the fairly short R_2 distances which signal the presence of such a bond. With respect to the nature of the acid substituents, the distance elongates in the order $SO_4 < CO_3 \ll 2Cl$. The β angle is roughly 180° for the NCH and NH_3 bases, placing the N equidistant between the two O atoms. However, the imine moves off this axis by quite a bit, which facilitates the formation of the CH···O H-bond. There is also a secondary H-bond in the case of $SpCl_2$, even without the need for the N to move off center. The α angles are commensurate with the central placement of the N atoms in all of the complexes, save those combining $NHCH_2$ with CO_3 or SO_4. With respect to the $SpCl_2$ units, they deform from their linear structure in the monomer to a bent configuration in the complex, as evidenced by the deviation of the α angles from 90°. The internal CO, SO, or SpCl bond length is defined as r_1 in Fig. 1. This bond undergoes a small stretch in the various complexes, denoted Δr_1 in Table 1. This stretch amounts to some 0.005 Å for most of the dyads, but is an order of magnitude larger within $SpCl_2$. These larger values arise as the Cl atoms are directly bonded to the Sp, rather than to C or S.

The last column of Table 1 contains the interaction energy of each base with the Lewis acid. These quantities are quite substantial, with a minimum of 12 kcal/mol and reaching all the way up to nearly 60 kcal/mol. The bonds are strongest for the imine base with its secondary interaction, and weakest for NCH with its sp-hybridization. Zn engages in stronger bonds than its Cd analogues, and the order with respect to ligands varies as $SpSO_4 > SpCO_3 \gg SpCl_2$. The greater strength of the Zn vs Cd spodium bonds is surprising in light of the trend in most other noncovalent bonds, e.g. halogen bonds, where a heavier electron donor atom is typically associated with a stronger bond [11].

Some insights into these trends may be gleaned by inspection of the molecular electrostatic potential (MEP) that surrounds each monomer. The MEP of each Lewis acid is characterized by a positive region directly along the X-Sp-X bisector, indicated by the red region in Fig. 2. This area corresponds to a σ-hole, and the magnitude of its MEP on the 0.001 au isodensity surface, denoted V_{max}, is displayed by the numbers in Fig. 2. This quantity is largest for the SO_4 ligand, followed by CO_3, and then by 2Cl much lower. This pattern reproduces the interaction energy trends in Table 1. Also consistent with the interaction energies, the Zn σ-holes are deeper than those for Cd. The only exception is $SpCl_2$ for which Cd has a slightly deeper σ-hole than Zn, contrary to E_{int}. With respect to the three bases, of most relevance is the blue minimum in the MEP at the N atom of NH_3 and $NHCH_2$ which have roughly the same V_{min}, with NCH somewhat less negative.

Like other related noncovalent bonds, the spodium bond is accompanied by a charge transfer (CT) from the electron donor molecule to the acceptor. This intermolecular transfer listed in Table 2 obeys many of the same patterns as the energetics. It is largest for $NHCH_2$, followed by NH_3, and then by NCH. Zn undergoes a larger CT than does Cd, and the ligand order follows the familiar $SpSO_4 > SpCO_3 \gg SpCl_2$. In fact, there is a fairly tight correlation between CT and E_{int}, as explicitly shown in Fig. 3 where there is a correlation coefficient $R^2 = 0.90$. The principal element of the charge transfer involves that from the base N lone pair to a vacant d-orbital on Sp. The orbitals involved, and their overlap, are visualized in Fig. S1. The energetic consequence of this inter-orbital transfer is listed in the last column of Table 2 as $E^{(2)}$. The magnitude of this quantity is fairly large, approaching 90 kcal/mol, signaling a strong interaction. Like the full CT, the trends are similar to that of the interaction energy: Zn > Cd, $NHCH_2 > NH_3 >$ NCH, and $SpSO_4 > SpCO_3 \gg SpCl_2$.

One can examine the shifts of electron density that accompany the formation of the spodium bond in different regions of space via an electron density difference map. This map in Fig. 4 subtracts the density of the two unperturbed monomers from that of the full dyad. The green regions in Fig. 4 indicate density gain while losses are depicted in orange. The pattern closely resembles those of related noncovalent bonds such as H-bonds, halogen bonds etc. There is a sizable gain in the region directly between the Zn and N atoms with orange losses closer to these two nuclei. The polarization within the NH_3 base that shifts density away from the three H atoms and toward the interacting N atom is

Table 1
Binding distances (R, Å), angles (α/β, deg), change of bond length (Δr_1, Å), and interaction energy (E_{int}, kcal/mol) in the spodium-bonded binary complexes.

	R_1	R_2	α	β	Δr_1	E_{int}
$ZnCO_3$-NCH(**1**)	1.912		142.4	179.8	0.006	−38.45
$ZnCO_3$-$NHCH_2$(**2**)	1.913	2.489	174.7	147.5	0.005	−53.45
$ZnCO_3$-NH_3(**3**)	1.948		143.0	179.8	0.006	−50.40
$CdCO_3$- NCH (**4**)	2.146		146.3	179.8	0.004	−31.84
$CdCO_3$-$NHCH_2$(**5**)	2.134	2.330	167.6	133.4	0.005	−45.01
$CdCO_3$-NH_3(**6**)	2.173		146.2	179.7	0.005	−43.50
$ZnSO_4$- NCH (**7**)	1.906		139.6	180.0	0.005	−42.55
$ZnSO_4$-$NHCH_2$(**8**)	1.905	2.449	171.1	148.2	0.005	−58.80
$ZnSO_4$-NH_3(**9**)	1.940		140.4	179.3	0.005	−55.25
$CdSO_4$- NCH (**10**)	2.135		143.6	179.9	0.004	−35.70
$CdSO_4$-$NHCH_2$(**11**)	2.104	2.324	172.0	135.2	0.004	−50.44
$CdSO_4$-NH_3(**12**)	2.144		144.4	179.3	0.005	−46.20
$ZnCl_2$- NCH (**13**)	2.154		103.7		0.044	−15.38
$ZnCl_2$-$NHCH_2$(**14**)	2.049	2.769	108.5		0.057	−30.73
$ZnCl_2$-NH_3(**15**)	2.080		106.5		0.061	−28.00
$CdCl_2$- NCH (**16**)	2.444		98.7		0.034	−12.07
$CdCl_2$-$NHCH_2$(**17**)	2.312	2.754	105.5		0.063	−23.96
$CdCl_2$-NH_3(**18**)	2.347		102.0		0.053	−21.30

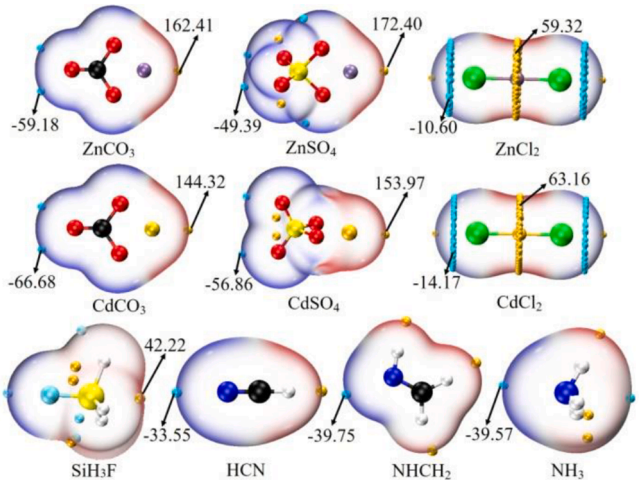

Fig. 2. MEP maps on the 0.001 electrons $Bohr^{-3}$ isodensity surface of monomers. Red and blue regions represent positive and negative MEPs, respectively. V_{max} and V_{min} in kcal/mol.

Table 2
Charge transfer (CT, e) and second-order perturbation energy ($E^{(2)}$, kcal/mol) for transfer from base N lone pair to unoccupied d-orbital of M in the spodium-bonded binary complexes.

	CT	$E^{(2)}$
$ZnCO_3$-NCH(**1**)	0.0497	64.06
$ZnCO_3$-$NHCH_2$(**2**)	0.0896	84.59
$ZnCO_3$-NH_3(**3**)	0.0834	84.17
$CdCO_3$- NCH (**4**)	0.0320	48.76
$CdCO_3$-$NHCH_2$(**5**)	0.0740	75.13
$CdCO_3$-NH_3(**6**)	0.0634	65.40
$ZnSO_4$- NCH (**7**)	0.0543	63.57
$ZnSO_4$-$NHCH_2$(**8**)	0.0939	88.02
$ZnSO_4$-NH_3(**9**)	0.0871	86.32
$CdSO_4$- NCH (**10**)	0.0362	51.12
$CdSO_4$-$NHCH_2$(**11**)	0.0818	81.60
$CdSO_4$-NH_3(**12**)	0.0733	77.86
$ZnCl_2$- NCH (**13**)	0.0217	24.58
$ZnCl_2$-$NHCH_2$(**14**)	0.0571	42.16
$ZnCl_2$-NH_3(**15**)	0.0481	38.10
$CdCl_2$- NCH (**16**)	0.0111	16.80
$CdCl_2$-$NHCH_2$(**17**)	0.0400	35.97
$CdCl_2$-NH_3(**18**)	0.0313	35.78

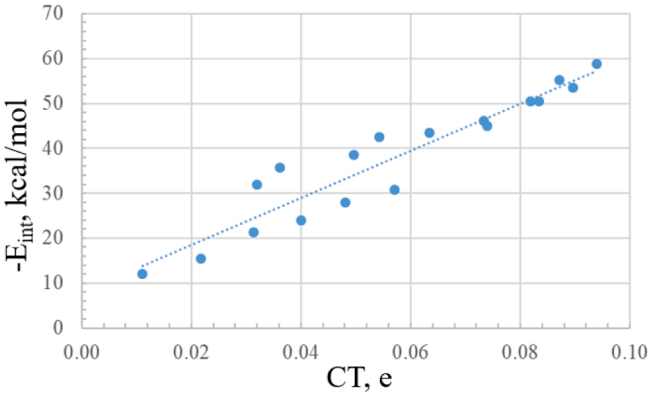

Fig. 3. Linear relationship between CT and E_{int} for the spodium-bonded dyads.

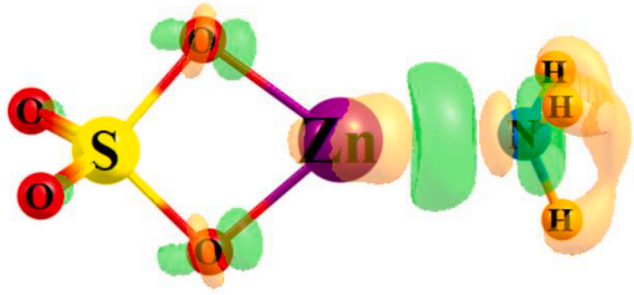

Fig. 4. Shifts of electron density accompanying formation of the $ZnSO_4$-NH_3 dimer. Contours shown are ± 0.005 a.u., where green and orange indicate gain and loss of density, respectively.

plainly visible by the orange areas around these three peripheral H atoms.

AIM analysis of the electron density offers another avenue by which to assess the strength of noncovalent interactions. The first columns of Table S1 contain the electron density (ρ), its Laplacian ($\nabla^2\rho$), and energy density (H) at the Sp•••N BCP (Fig. S2). The density varies from 0.04 a.u. to 0.1 a.u. and exhibits a strong correlation with the binding distance, excluding $SpCO_3$/$SpSO_4$-NCH (Fig. S3). $\nabla^2\rho$ lies in the 0.16–0.46 a.u. range but is not well correlated with the strength of the spodium bond. The large ρ in the neighborhood of 0.1 a.u., positive $\nabla^2\rho$ and negative H are indicative of a spodium bond that is at least partially covalent. This conclusion is further confirmed by the ratio of absolute potential energy density (|V|) to the kinetic energy density (G), which is somewhat greater than unity at 1.07–1.31. Related to AIM is the NCI analysis of the total electron density. The NCI diagrams of the Zn-bonded dyads are presented in Fig. S4 which confirm the formation of spodium bonds, as well as the secondary interactions involving the imine. The spodium bond is clearly evident by the blue regions, while the areas signaling the CH···O/Cl secondary interactions are green, indicating weaker bonds.

Another tool by which to understand the forces comprising a noncovalent bond is a decomposition of its interaction energy into separate components: electrostatic (E^{es}), exchange (E^{ex}), repulsive (E^{rep}), polarization (E^{pol}) and dispersion (E^{disp}) (Table S2). A shorter Sp•••N distance causes a larger E^{rep}, which is counteracted by a stronger orbital exchange attraction E^{ex}. Attention is focused here on the three principal attractive terms, plotted in Fig. 5. E^{es} is larger than E^{pol} which is in turn larger than E^{disp}. In quantitative terms, E^{pol} amounts to 40–60% of E^{es}. Thus the spodium bond is composed largely of electrostatic attraction, complemented by a sizable polarization element.

3.2. Tetrel-bonded binary complexes

As is clear from Fig. 2, the O atoms of $SpCO_3$/$SpSO_4$ and the Cl atoms of $SpC1_2$ are surrounded by negative blue regions, so ought to be attracted to the positive region of a neighboring molecule. SiH_3F offers such a positive region in the form of a σ-hole on the central Si atom, along the extension of the F-Si bond axis. Indeed, all of the various metal-containing molecules engage in such a Si···O/Cl tetrel bond, as detailed in the geometries of Fig. 6, wherein R_3 refers to the Si···O/Cl intermolecular distance. (It is important for the following narrative to understand that the various Sp-containing molecules that acted as Lewis acid in the spodium bond reverse their role to that of base in the tetrel bonds.)

This distance is reported in Table 3, along with other aspects of the equilibrium geometries and the interaction energy in the last column. The Si···O distances are all shorter than Si···Cl, sensible in light of the smaller atomic radius of O. These Si···O distances are also shorter for Cd as compared to Zn, which is consistent with the more negative V_{min} on the O atoms for the former in Fig. 2. The γ angles are all close to 180°, which support the character of these interactions as tetrel bonds. As indicated in the next two columns of Table 3, the internal bonds of both acid and base molecules are stretched by the interaction, particularly those within the acid. The interaction energies of these tetrel bonds range between 3 kcal/mol for the Si···Cl bonds up to nearly 10 kcal/mol for Si···O. These bonds are stronger for Sp = Cd than for Zn, again consistent with V_{min} depths on the O atoms. On the other hand, the

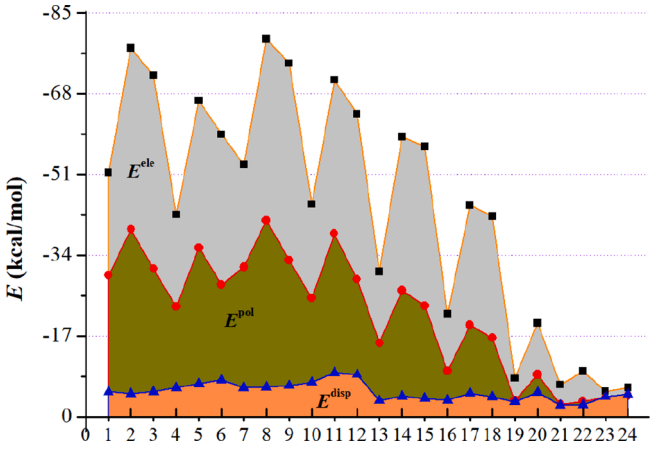

Fig. 5. Electrostatic (gray), polarization (green) and dispersion (yellow) energies in the binary complexes.

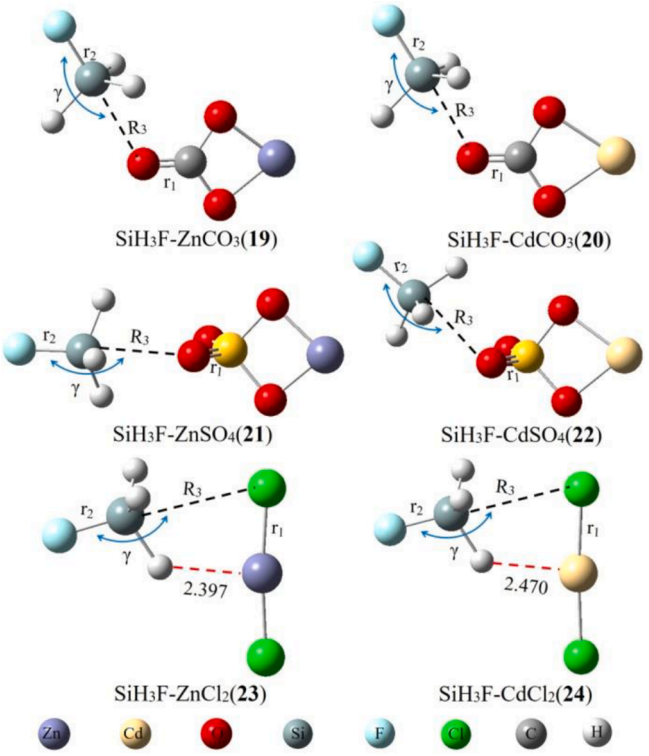

Fig. 6. Optimized geometries of tetrel-bonded binary complexes.

Table 3
Binding distance (R, Å), angles (γ, deg), change of bond length (Δr, Å), and interaction energy (E_{int}, kcal/mol) in the tetrel-bonded binary complexes.

	R_3	γ	Δr_1	Δr_2	E_{int}
SiH_3F-$ZnCO_3$(**19**)	2.612	178.9	0.008	0.021	−7.09
SiH_3F-$CdCO_3$(**20**)	2.503	178.8	0.010	0.028	−9.13
SiH_3F-$ZnSO_4$(**21**)	2.813	177.5	0.006	0.014	−4.72
SiH_3F-$CdSO_4$(**22**)	2.741	178.0	0.007	0.017	−5.71
SiH_3F-$ZnCl_2$(**23**)	3.379	174.4	0.014	−0.002	−2.72
SiH_3F-$CdCl_2$(**24**)	3.381	175.9	0.008	−0.002	−3.28

$SpCO_3$ base engages in stronger tetrel bonds than $SpSO_4$, although it is the latter that is associated with larger V_{min}.

The overall charge transfer CT is smaller in these tetrel bonds than for the spodium bonds, revealed by comparison of Table 4 with Table 2. The principal interorbital interaction within the tetrel bonds involves transfer from the O/Cl lone pair to the σ*(Si-F) antibonding orbital. Table 4 shows that $E^{(2)}$ for this transfer lies in the 4–8 kcal/mol range, an order of magnitude smaller than in the spodium bonds. There is also evidence of a weak SiH···O/Cl interaction, particularly Cl, as documented by the transfers from the σ(Si-H) orbital to the indicated σ* orbital of the base.

Both the electron density and its Laplacian at the Si•••O/Cl BCP (Table S3) show a pattern that is consistent with the interaction energy.

Table 4
Charge transfer (CT, e) and second-order perturbation energies ($E^{(2)}$, kcal/mol) in the tetrel-bonded binary complexes.

	CT		$E^{(2)}$		$E^{(2)}$
SiH_3F-$ZnCO_3$(**19**)	0.0310	$LP_O \rightarrow \sigma^*_{Si\text{-}F}$	6.32	$\sigma_{Si\text{-}H} \rightarrow \sigma^*_{C\text{-}O}$	0.10
SiH_3F-$CdCO_3$(**20**)	0.0415	$LP_O \rightarrow \sigma^*_{Si\text{-}F}$	7.56	$\sigma_{Si\text{-}H} \rightarrow \sigma^*_{C\text{-}O}$	0.20
SiH_3F-$ZnSO_4$(**21**)	0.0167	$LP_O \rightarrow \sigma^*_{Si\text{-}F}$	3.67	$\sigma_{Si\text{-}H} \rightarrow \sigma^*_{S\text{-}O}$	0.11
SiH_3F-$CdSO_4$(**22**)	0.0176	$LP_O \rightarrow \sigma^*_{Si\text{-}F}$	3.70	$\sigma_{Si\text{-}H} \rightarrow \sigma^*_{S\text{-}O}$	0.13
SiH_3F-$ZnCl_2$(**23**)	0.0053	$LP_{Cl} \rightarrow \sigma^*_{Si\text{-}F}$	3.57	$\sigma_{Si\text{-}H} \rightarrow \sigma^*_{Cl\text{-}Zn}$	1.43
SiH_3F-$CdCl_2$(**24**)	0.0098	$LP_{Cl} \rightarrow \sigma^*_{Si\text{-}F}$	3.59	$\sigma_{Si\text{-}H} \rightarrow \sigma^*_{Cl\text{-}Cd}$	2.56

The BCP densities are much smaller here than in the spodium bonds, all 0.02 a.u. or less. The density Laplacian is consistently positive, but again much smaller than in the spodium bonds. The stronger tetrel bond in SiH_3F-$SpCO_3$ is characterized by a negative energy density, while this quantity is positive in the other tetrel-bonded complexes. Although the tetrel bond in SiH_3F-$SpCO_3$ has a partially covalent property, it is still dominated by electrostatic energy (Fig. 5 and Table S2). This electrostatic dominance is also found in SiH_3F-$SpSO_4$. The three attractive terms (E^{es}, E^{pol}, and E^{disp}) are comparable in SiH_3F-$SpCl_2$.

In summary, the tetrel bonds involving $SiFH_3$ are all typical sorts of noncovalent bonds, but are much weaker than the spodium bonds achieved when the Sp-containing molecules are combined with any of the various *N*-containing bases.

3.3. Cooperativity between spodium and tetrel bonds

As the central metal-bearing molecule serves as an electron donor in its spodium bond with a base, and as an acceptor when it engages in a tetrel bond with $SiFH_3$, one might anticipate that the two bonds ought to strengthen one another if both are present. The optimized geometries of these ternary complexes are compiled in Fig. 7 where most of them closely retain the central features present in each dyad. The exception to this resemblance arises in those containing $SpCl_2$. These triads place the $SiFH_3$ well out of the plane containing the other two molecules.

Table 5 lists the energetics of the ternary complexes where it may be noted first that the total interaction energy varies between −17 and −66 kcal/mol. It is of interest to examine how this total compares with the individual noncovalent bonding interactions. ΔE_{TB}, for example, considers the tetrel bond interaction energy between $SiFH_3$ and the SpL_2:*N*-base pair within the geometry adopted within the triad. Likewise, ΔE_{SpB} evaluates the interaction between $SiFH_3$:SpL_2 and the *N*-base. For purposes of completeness, the interaction energy between $SiFH_3$ and the *N*-base is listed in Table 5 as ΔE_{far}, which are of course small in magnitude since these two subunits are some distance from one another.

The interaction energies of both tetrel and spodium bonds are more negative in the ternary complexes than in the dyads, indicating these bonds mutually reinforce one another in what is termed positive cooperativity. The amounts by which each bond is strengthened by the presence of the other are listed as $\Delta\Delta E_{TB}$ and $\Delta\Delta E_{SpB}$ in Table 5, and are as large as 6 kcal/mol in some cases. On a percentage basis, the TB is enhanced more than is the SpB, suggesting the strong polarizing effect of the SpB. Indeed, the interaction energy of the TB rises up to −15 kcal/mol in SiH_3F-$CdCO_3$-NH_3, rather larger than the bulk of tetrel bonds in the literature.

One can quantify the degree of cooperativity by E_{coop} in the last column of Table 5, which relates the total interaction energy in the triad to the sum of TB and SpB optimized dyads, plus ΔE_{far} to account for the small interactions between $SiFH_3$ and the *N*-base within the triad. The negative values of E_{coop} reaffirm the positive cooperativity wherein the two noncovalent bonds reinforce one another. On a percentage basis, E_{coop} represents between 1 and 10% of the total triad interaction energy.

The cooperativity manifests itself in other aspects of these triads. The presence of the TB shortens the intermolecular distance within the SpB, and vice versa, as shown in the negative values of ΔR_1 and ΔR_3 in Table S4. As in the case of the energetics, the TB undergoes a greater degree of bond contraction than does the SpB. For example, the shortening of Si•••O/Cl distance is larger than 0.1 Å in most ternary complexes, while the contraction of the Sp•••N distance is less than 0.03 Å. In addition, the electron densities at the Si•••O/Cl and Sp•••N BCPs are also increased in the ternary complexes, relative to their values in the dyads. Table S5 documents the increases in the intermolecular charge transfers arising from addition of the third molecule to each dyad. The largest charge transfer is 0.07 e for the tetrel bond and 0.10 e for the spodium bond.

Since the electrostatic term has been shown above to be quite important for both the SpB and TB, it was informative to examine how

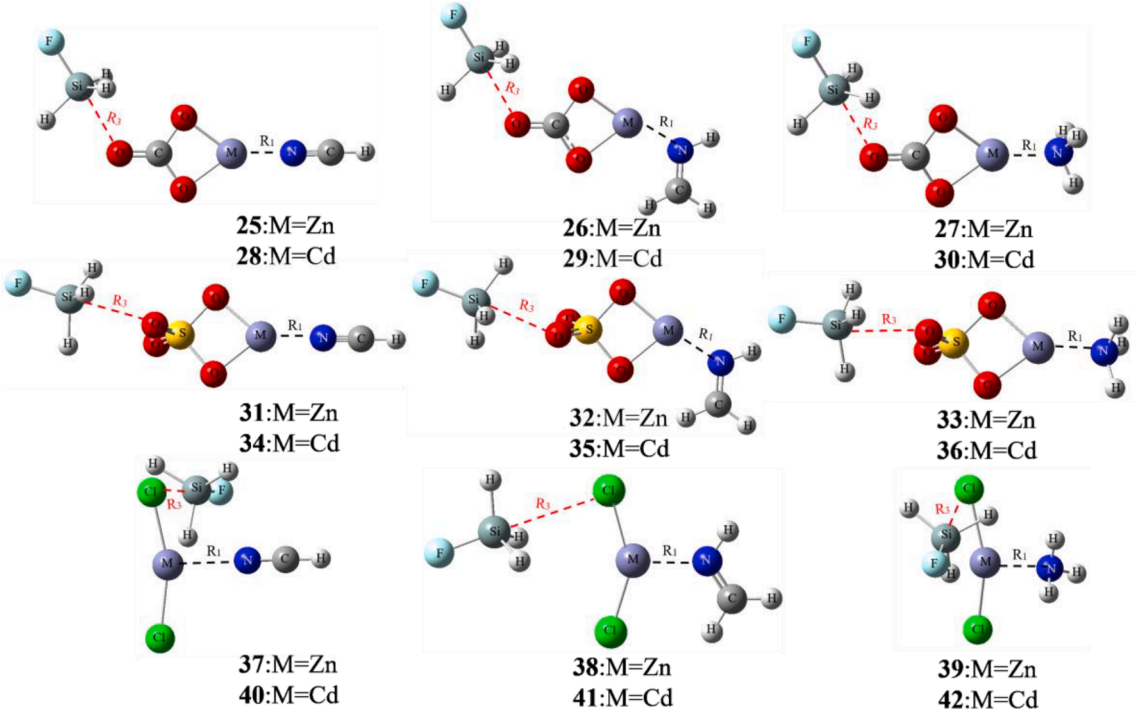

Fig. 7. Optimized geometries of ternary complexes.

Table 5
Total interaction energy (ΔE_{total}), interaction energy between molecular pairs (ΔE), and cooperative energy (E_{coop}) in the ternary complexes, all in kcal/mol.

	ΔE_{total}	ΔE_{TB}	ΔE_{SpB}	ΔE_{far}	$\Delta\Delta E_{TB}$	$\Delta\Delta E_{SpB}$	E_{coop}
SiH_3F-$ZnCO_3$-HCN(25)	−50.22	−11.45	−41.54	−0.29	−4.36	−3.09	−4.39
SiH_3F-$ZnCO_3$-$NHCH_2$(26)	−65.41	−11.68	−56.58	−0.23	−4.59	−3.13	−4.64
SiH_3F-$ZnCO_3$-NH_3(27)	−62.83	−12.03	−53.88	−0.26	−4.94	−3.48	−5.08
SiH_3F-$CdCO_3$-HCN(28)	−46.13	−14.13	−34.85	−0.26	−5.00	−3.01	−4.90
SiH_3F-$CdCO_3$-$NHCH_2$(29)	−58.69	−14.89	−47.16	−0.24	−5.76	−2.15	−4.31
SiH_3F-$CdCO_3$-NH_3(30)	−58.83	−15.07	−47.13	−0.23	−5.94	−3.63	−5.97
SiH_3F-$ZnSO_4$-HCN(31)	−49.82	−7.13	−44.18	−0.21	−2.41	−1.63	−2.34
SiH_3F-$ZnSO_4$-$NHCH_2$(32)	−66.23	−6.96	−60.77	−0.16	−2.24	−1.97	−2.55
SiH_3F-$ZnSO_4$-NH_3(33)	−64.94	−7.04	−59.51	−0.16	−2.32	−4.26	−4.81
SiH_3F-$CdSO_4$-HCN(34)	−43.84	−8.11	−37.15	−0.19	−2.40	−1.45	−2.24
SiH_3F-$CdSO_4$-$NHCH_2$(35)	−58.90	−7.79	−52.39	−0.12	−2.08	−1.95	−2.63
SiH_3F-$CdSO_4$-NH_3(36)	−55.39	−8.19	−48.72	−0.15	−2.48	−2.52	−3.33
SiH_3F-$ZnCl_2$-HCN(37)	−20.53	−4.38	−16.98	−0.89	−1.66	−1.60	−1.54
SiH_3F-$ZnCl_2$-$NHCH_2$(38)	−34.74	−3.37	−32.46	−0.39	−0.65	−1.73	−0.90
SiH_3F-$ZnCl_2$-NH_3(39)	−33.22	−4.37	−29.84	−0.69	−1.65	−1.84	−1.81
SiH_3F-$CdCl_2$-HCN(40)	−16.97	−4.62	−13.21	−0.97	−1.34	−1.14	−0.65
SiH_3F-$CdCl_2$-$NHCH_2$(41)	−27.27	−3.61	−24.72	−0.35	−0.33	−0.76	−0.18
SiH_3F-$CdCl_2$-NH_3(42)	−26.45	−4.66	−22.61	−0.72	−1.38	−1.31	−1.15

the formation of each such bond affects the σ-hole or σ-lump that is key to the formation of the other bond. As a specific example, $V_{S,min}$ on the O atoms of $ZnCO_3$ is of course important to the formation of a TB with $SiFH_3$. The first entries in Table 6 show that $V_{S,min}$ is equal to −73.14 kcal/mol in the $ZnCO_3$-NCH dyad, 13.96 kcal/mol more negative than its value within the $ZnCO_3$ monomer. Indeed, the addition of each *N*-base adds to the negative value of the MEP on the relevant atom of the Sp-bearing molecule, thus enabling the formation of a stronger TB with $SiFH_3$. The right side of Table 6 displays the alternate view, of how the addition of the $SiFH_3$ molecule adds to the σ-hole on the Sp atom, enabling a strengthened SpB. Note that the latter σ-hole enhancements are smaller than the σ-lump magnifications on the left side of Table 6, consistent with the greater strengthening of the TB as compared to the SpB in the triads.

4. Discussion and conclusions

The spodium bonds in the systems examined here are quite strong. The interaction energies approach 60 kcal/mol in some cases, with even the weakest equal to 12 kcal/mol. Noncovalent bonds of such strength are not very common, particularly as neither subunit carries a charge. The bicoordinated Sp atom is studied in the spodium bonds reported here, thus it is interesting to compare with the tri or tetracoordinated situations. The interaction energy is 21.9 kcal/mol for the dimer [Hg(HL)I_2]$_2$ (HL = N'-(3-nitrobenzylidene)isonicotinohydrazide), wherein a hydrogen bond, spodium bond, and π-π interaction are all present [64]. For the SpX_2L_2 (X = Cl, Br or I; L = thiurea) adducts with carbon monoxide, acetonitrile, formaldehyde, or methanethial, the interaction energy is less than 10 kcal/mol.[14] Obviously, the bicoordinated Sp atom engages in a much stronger spodium bond than the tri or tetracoordinated species. Even the binding of the CN^- anion with the tricoordinated Sp atom in $SpCl_3^-$ is very weak [65]. The interaction energy is 16 kcal/

Table 6
The most negative MEP ($V_{S,min}$) on the O/Cl atom in the spodium-bonded complexes, the most positive MEP ($V_{S,max}$) on the M atom in the tetrel-bonded complexes, and their difference (ΔV) relative to the isolated molecule, all in kcal/mol.

	$V_{S,min}$	$\Delta V_{S,min}$		$V_{S,max}$	$\Delta V_{S,max}$
$ZnCO_3$-NCH(**1**)	−73.14	−13.96	SiH_3F-$ZnCO_3$(**19**)	171.57	9.16
$ZnCO_3$-$NHCH_2$(**2**)	−72.51	−13.33	SiH_3F-$CdCO_3$(**20**)	153.26	8.94
$ZnCO_3$-NH_3(**3**)	−72.26	−13.08	SiH_3F-$ZnSO_4$(**21**)	178.71	6.31
$CdCO_3$- NCH(**4**)	−78.38	−11.70	SiH_3F-$CdSO_4$(**22**)	159.40	5.43
$CdCO_3$-$NHCH_2$(**5**)	−77.61	−10.93	SiH_3F-$ZnCl_2$(**23**)	63.97	4.65
$CdCO_3$-NH_3(**6**)	−78.14	−11.46	SiH_3F-$CdCl_2$(**24**)	66.23	3.07
$ZnSO_4$- NCH(**7**)	−63.68	−14.29			
$ZnSO_4$-$NHCH_2$(**8**)	−62.47	−13.08			
$ZnSO_4$-NH_3(**9**)	−62.72	−13.33			
$CdSO_4$- NCH(**10**)	−68.77	−11.91			
$CdSO_4$-$NHCH_2$(**11**)	−66.63	−9.77			
$CdSO_4$-NH_3(**12**)	−68.12	−11.26			
$ZnCl_2$- NCH(**13**)	−27.46	−16.86			
$ZnCl_2$-$NHCH_2$(**14**)	−29.63	−19.03			
$ZnCl_2$-NH_3(**15**)	−27.26	−16.66			
$CdCl_2$- NCH(**16**)	−27.26	−13.09			
$CdCl_2$-$NHCH_2$(**17**)	−28.94	−14.77			
$CdCl_2$-NH_3(**18**)	−27.08	−12.91			

mol in $HgCl_2$-NMe_3 [66], where NMe_3 is a better electron donor than NH_3, while the interaction energy is larger than 20 kcal/mol when $ZnCl_2$ or $CdCl_2$ binds with NH_3. Apparently $HgCl_2$ participates in a weaker spodium bond than $ZnCl_2$ or $CdCl_2$. When carbenes act as the electron donors [67], the spodium bonds are stronger than those with $NHCH_2$.

Another measure of the strength of these bonds is the high degree of charge transferred from the base molecule to the acid, as high as 0.08 e. Along with this overall transfer is the component that involves the N lone pair and the relevant d-orbital of the metal, for which $E^{(2)}$ reaches to nearly 90 kcal/mol in some cases. Moreover, the AIM bond critical point density is in the range of 0.1 a.u., and H is uniformly negative by as much as −0.05 a.u.. All of these markers place this spodium bond on the borderline between noncovalent and covalent bonds. From another perspective, the intermolecular R(Sp···N) distance is rather short, hovering in the 1.9–2.4 Å range. This bond is only slightly longer than the internal Sp-O bonds within the Lewis acids, by between 0.05 and 0.13 Å.

Given these measures of bond strength, it might be possible to categorize these spodium bonds as coordinate covalent bonds. In order to address this issue, AIM parameters were used to directly compare these spodium and coordinate covalent bonds within the same species. Like the spodium bond, the Sp-O/Cl coordinate covalent bonds are marked by a large electron density, positive Laplacian, and negative energy density (Table S6). On the other hand, these quantities are generally somewhat smaller in magnitude for the spodium bonds. The spodium BCP densities, for example, are between 43 and 99% the size of the coordinate bonds; $\nabla^2\rho$ varies between 68 and 108%. NCI analysis shows similar features for both the spodium bond and coordinate covalent bonds (Fig. S4). A red circle is present between the Sp-O/Cl bond and Sp-N bond.

The BSSE correction amounts to 0.85–1.52 kcal/mol (Table S2). It is small in magnitude, but its effect on the interaction energy is different for the SpB and TB interactions. BSSE is equal to 2–8% of the SpB interaction energy and 11–34% of the TB interaction energy. Thus the BSSE correction represents a larger proportion for the weak interactions.

In conclusion, the spodium bonds considered here are quite strong, with interaction energies approaching 60 kcal/mol. Those involving Zn are a bit stronger than its heavier Cd congener. The ditopic SO_4 ligand provides the strongest binding, followed closely by CO_3, whereas the two separate Cl ligands result in a considerably weaker spodium bond. NCH is the weakest of the three bases considered, but even so its spodium bonds exceed 12 kcal/mol. Tetrel bonds between the Si of SiH_3F and the O or Cl atom of the ligand on the spodium atom are of moderate strength, between 3 and 9 kcal/mol. When present in tandem the spodium and tetrel bonds reinforce one another. The larger perturbations of the electronic structure caused by the spodium bond result in a greater strengthening of the tetrel bond than vice versa.

CRediT authorship contribution statement

Na Liu: Data curation, Visualization, Investigation, Writing – original draft. **Qingzhong Li:** Methodology, Software. **Steve Scheiner:** Supervision.

Declaration of Competing Interest

The authors declare that they have no known competing financial interests or personal relationships that could have appeared to influence the work reported in this paper.

Acknowledgements

This work was supported by the Natural Science Foundation of Shandong Province (ZR2021MB123) and by the US National Science Foundation (1954310).

Appendix A. Supplementary data

Supplementary data to this article can be found online at https://doi.org/10.1016/j.chemphys.2022.111470.

References

[1] G. Chalasiński, M.M. Szczeniak, State of the art and challenges of the ab initio theory of intermolecular interactions, Chem. Rev. 100 (2000) 4227–4252.
[2] S. Nieto, A.E. Hargrove, T. Zhang, J.L. Sessler, E.V. Anslyn, Artificial receptors for the recognition of phosphorylated molecules, Chem. Rev. 111 (2011) 6603–6782.
[3] D.M. Rudkevich, Emerging supramolecular chemistry of gases, Angew. Chem. Int. Ed. 43 (5) (2004) 558–571.
[4] H. Wang, H.K. Bisoyi, A.M. Urbas, T.J. Bunning, Q. Li, The halogen bond: An emerging supramolecular tool in the design of functional mesomorphic materials, Chem. Eur. J. 25 (2019) 1369–1378.
[5] L. Catalano, S. Perez-Estrada, G. Terraneo, T. Pilati, G. Resnati, P. Metrangolo, M. A. Garcia-Garibay, Dynamic characterization of crystalline supramolecular rotors assembled through halogen bonding, J. Am. Chem. Soc. 137 (2015) 15386–15389.
[6] H.T. Le, C.G. Wang, A. Goto, Solid-phase radical polymerization of halogen-bond-based crystals and applications to pre-shaped polymer materials, Angew. Chem. Int. Ed. 59 (2020) 9360–9364.
[7] Y.-C. Chan, Y.-Y. Yeung, Halogen bond catalyzed bromocarbocyclization, Angew. Chem. Int. Ed. 57 (13) (2018) 3483–3487.
[8] L. Carreras, M. Serrano-Torné, P.W. van Leeuwen, A. Vidal-Ferran, XBphos-Rh: A halogen-bond assembled supramolecular catalyst, Chem. Sci. 9 (2018) 3644–3648.
[9] P. Molina, F. Zapata, A. Caballero, Anion recognition strategies based on combined noncovalent interactions, Chem. Rev. 117 (2017) 9907–9972.
[10] K.J. Donald, B.K. Wittmaack, C. Crigger, Tuning σ-holes: Charge redistribution in the heavy (group 14) analogues of simple and mixed halomethanes can impose strong propensities for halogen bonding, J. Phys. Chem. A 114 (2010) 7213–7222.
[11] T. Clark, M. Hennemann, J.S. Murray, P. Politzer, Halogen bonding: The σ-hole, J. Mol. Model. 13 (2) (2007) 291–296.
[12] P. Politzer, J.S. Murray, M.C. Concha, Electrostatically driven complexes of SiF_4 with amines, Int. J. Quant. Chem. 109 (2009) 3773–3780.
[13] J.S. Murray, P. Lane, P. Politzer, Expansion of the σ-hole concept, J. Mol. Model. 15 (2009) 723–729.
[14] A. Bauzá, I. Alkorta, J. Elguero, T.J. Mooibroek, A. Frontera, Spodium bonds: Noncovalent interactions involving group 12 elements, Angew. Chem. Int. Ed. 59 (2020) 17482–17487.
[15] C. Chieh, Synthesis and structure of dichlorobis (thiosemicarbazide) mercury (II), Can. J. Chem. 55 (1977) 1583–1587.
[16] A.J. Lupinetti, V. Jonas, W. Thiel, S.H. Strauss, G. Frenking, Trends in molecular geometries and bond strengths of the homoleptic $^{d1}0$ metal carbonyl cations [M $(CO)n]^{lx}_{+}$ $^{(M}x{+=}^{C}u{+}$, $^{A}g{+}$, $^{A}u{+}$, $^{Zn}2{+}$, $^{Cd}2{+}$, $^{Hg}2{+}$; n=1–6): A theoretical study, Chem. Eur. J. 5 (9) (1999) 2573–2583.
[17] S.R. Wang, M. Arrowsmith, H. Braunschweig, R.D. Dewhurst, M. Dömling, J. D. Mattock, C. Pranckevicius, A. Vargas, Monomeric 16-electron π-diborene complexes of Zn (II) and Cd (II), J. Am. Chem. Soc. 139 (2017) 10661–10664.

[18] M.R. Porter, S.E. Lindahl, A. Lietzke, E.M. Metzger, Q. Wang, E. Henck, C.-H. Chen, H. Niu, J.M. Zaleski, Metal-mediated diradical tuning for DNA replication arrest via template strand scission, Proc. Natl. Acad. Sci. USA 114 (36) (2017) E7405–E7414.

[19] L.-B. Yang, H.-C. Wang, A.-N. Dou, M.-Z. Rong, A.-X. Zhu, Z. Yang, Roles of anions in the structural diversity of Cd(II) complexes based on a V-shaped triazole-carboxylate ligand: Synthesis, structure and photoluminescence properties, Inorg. Chim. Acta 446 (2016) 103–110.

[20] K.B. Borisenko, R.O. Gould, C.A. Morrison, A theoretical and experimental study of weak silane–electron donor interactions, J. Mol. Struct. 554 (2000) 163–172.

[21] I. Alkorta, I. Rozas, J. Elguero, Molecular complexes between silicon derivatives and electron-rich groups, J. Phys. Chem. A 105 (2001) 743–749.

[22] S. Scheiner, Noncovalent Forces, Springer, 2015.

[23] M.A.A. Ibrahim, A.A.K. Kamel, M.E.S. Soliman, M.F. Moustafa, H.R.A. El-Mageed, F. Taha, L.A. Mohamed, N.A.M. Moussa, Effect of external electric field on tetrel bonding interactions in (FTF_3···FH) complexes (T = C, Si, Ge, and Sn), ACS Omega 6 (39) (2021) 25476–25485.

[24] M.A.A. Ibrahim, N.A.M. Moussa, M.E.S. Soliman, M.F. Moustafa, J.H. Al-Fahemi, H.R.A. El-Mageed, On the potentiality of X-T-X_3 compounds (T = C, Si, and Ge, and X = F, Cl, and Br) as tetrel- and halogen-bond donors, ACS Omega 29 (2021) 19330–19341.

[25] M.A.A. Ibrahim, O.A.M. Ahmed, N.A.M. Moussa, S. El-Taher, H. Moustafa, Comparative investigation of interactions of hydrogen, halogen and tetrel bond donors with electron-rich and electron-deficient π-systems, RSC Adv. 9 (2019) 32811–32820.

[26] A. Bauzá, J. Tiddo, T.J. Mooibroek, A. Frontera, Tetrel-bonding interaction: Rediscovered supramolecular force? Angew. Chem. Int. Ed. 125 (2013) 12543–12547.

[27] N.W. Mitzel, A.J. Blake, D.W.H. Rankin, β-Donor bonds in SiON units: An inherent structure-determining property leading to (4 + 4)-coordination in tetrakis-(N, N-dimethylhydroxylamido)silane, J. Am. Chem. Soc. 119 (1997) 4143–4148.

[28] A. Bundhun, P. Ramasami, J.S. Murray, P. Politzer, Trends in σ-hole strengths and interactions of F_3MX molecules (M= C, Si, Ge and X= F, Cl, Br, I), J. Mol. Model. 19 (7) (2013) 2739–2746.

[29] D. Mani, E. Arunan, The X-C···Y (X = O/F, Y = O/S/F/Cl/Br/N/P) 'carbon bond' and hydrophobic interactions, Phys. Chem. Chem. Phys. 15 (2013) 14377–14383.

[30] K.J. Donald, M. Tawfik, The weak helps the strong: Sigma-holes and the stability of MF_4·base complexes, J. Phys. Chem. A 117 (2013) 14176–14183.

[31] S. Scheiner, Comparison of CH···O, SH···O, chalcogen, and tetrel bonds formed by neutral and cationic sulfur-containing compounds, J. Phys. Chem. A 119 (2015) 9189–9199.

[32] D. Mani, E. Arunan, The X-C···π (X= F, Cl, Br, Cn) carbon bond, J. Phys. Chem. A 118 (43) (2014) 10081–10089.

[33] Q.-Z. Li, H.-Y. Zhuo, H.-B. Li, Z.-B. Liu, W.-Z. Li, J.-B. Cheng, Tetrel–hydride interaction between XH_3F (X = C, Si, Ge, Sn) and HM (M = Li, Na, BeH, MgH), J. Phys. Chem. 119 (11) (2015) 2217–2224.

[34] M.D. Esrafili, F. Mohammadian-Sabet, Exploring σ-hole bonding in XH_3Si···HMY (X= H, F, CN; M= Be, Mg; Y= H, F, CH_3) complexes: A "tetrel-hydride" interaction, J. Mol. Model. 21 (2015) 60.

[35] Q.Z. Li, X. Guo, X. Yang, W.Z. Li, J.B. Cheng, A σ-hole interaction with radical species as electron donors: Does single-electron tetrel bonding exist? Phys. Chem. Chem. Phys. 16 (2014) 11617–11625.

[36] M.X. Liu, Q.Z. Li, W.Z. Li, J.B. Cheng, Carbene tetrel-bonded complexes, Struct. Chem. 28 (2017) 823–831.

[37] J.E. Del Bene, I. Alkorta, J. Elguero, Carbenes as electron-pair donors To CO_2 for C···C tetrel bonds and C-C covalent bonds, J. Phys. Chem. A 121 (2017) 4039–4047.

[38] Q.J. Tang, Q.Z. Li, Interplay between tetrel bonding and hydrogen bonding interactions in complexes involving F_2XO (X= C and Si) and HCN, Comput. Theor. Chem. 1050 (2014) 51–57.

[39] M. Solimannejad, S. Amani, M. Orojloo, Effect of cooperativity in lithium bonding on the strength of halogen bonding and tetrel bonding: $(LiCN)_n$···$ClYF_3$ and $(LiCN)_n$···YF_3Cl (Y= C, Si and n = 1–5) complexes as a working model, J. Mol. Model. 21 (2015) 183.

[40] X. Guo, Y.W. Liu, Q.Z. Li, W.Z. Li, J.B. Cheng, Competition and cooperativity between tetrel bond and chalcogen bond in complexes involving F_2CX (X= Se and Te), Chem. Phys. Lett. 620 (2015) 7–12.

[41] M.D. Esrafili, N. Mohammadirad, M. Solimannejad, Tetrel bond cooperativity in open-chain $(CH_3CN)_n$ and $(CH_3NC)_n$ clusters (n= 2–7): An ab initio study, Chem. Phys. Lett. 628 (2015) 16–20.

[42] M.D. Esrafili, R. Nurazar, F. Mohammadian-Sabet, Cooperative effects between tetrel bond and other σ–hole bond interactions: A comparative investigation, Mol. Phys. 113 (2015) 3703–3711.

[43] K. Kuwajima, The molten globule state as a clue for understanding the folding and cooperativity of globular-protein structure, Proteins 6 (1989) 87–103.

[44] L. Krbek, C.A. Schalley, P. Thordarson, Assessing cooperativity in supramolecular systems, Chem. Soc. Rev. 46 (2017) 2622–2637.

[45] L. Tebben, C. Mück-Lichtenfeld, G. ernández, S. Grimme, A. Studer, From additivity to cooperativity in chemistry: Can cooperativity be measured? Eur. J. Chem. 23 (2017) 5864–5873.

[46] H. Zhou, H. Dang, J.-H. Yi, A. Nanci, A. Rochefort, J.D. Wuest, Frustrated 2D molecular crystallization, J. Am. Chem. Soc. 129 (45) (2007) 13774–13775.

[47] K.L. Schuchardt, B.T. Didier, T. Elsethagen, L. Sun, V. Gurumoorthi, J. Chase, T. L. Windus, Basis set exchange: A community database for computational sciences, J. Chem. Inf. Model. 47 (2007) 1045–1052.

[48] A.S. Novikov, M.L. Kuznetsov, Theoretical study of Re (IV) and Ru (II) bis-isocyanide complexes and their reactivity in cycloaddition reactions with nitrones, Inorg. Chim. Acta 380 (2012) 78–89.

[49] A.A. Melekhova, A.S. Novikov, K.V. Luzyanin, N.A. Bokach, G.L. Starova, V. V. Gurzhiy, V.Y. Kukushkin, Tris-isocyanide copper (I) complexes: Synthetic, structural, and theoretical study, Inorg. Chim. Acta 434 (2015) 31–36.

[50] T.B. Anisimova, M.A. Kinzhalov, M.F.C.G. da Silva, A.S. Novikov, V.Y. Kukushkin, A.J. Pombeiro, K.V. Luzyanin, Addition of N-nucleophiles to gold (III)-bound isocyanides leading to short-lived gold (III) acyclic diaminocarbene complexes, New J. Chem. 41 (2017) 3246–3250.

[51] A.N. Usoltsev, S.A. Adonin, A.S. Novikov, D.G. Samsonenko, M.N. Sokolov, V. P. Fedin, One-dimensional polymeric polybromotellurates (IV): Structural and theoretical insights into halogen··· halogen contacts, CrystEngComm 19 (2017) 5934–5939.

[52] S.A. Adonin, A.S. Novikov, M.N. Sokolov, Polymeric lead (II) iodoacetate: Pb···I and I···I non-covalent interactions in the solid state, Eur. J. Inorg. Chem. 2019 (2019) 4221–4223.

[53] A.V. Chupina, V. Shayapov, A.S. Novikov, V.V. Volchek, E. Benassi, P.A. Abramov, M.N. Sokolov, $[\{AgL\}_2Mo_8O_{26}]_n$–complexes: A combined experimental and theoretical study, Dalton Trans. 49 (2020) 1522–1530.

[54] S.F. Boys, F. Bernardi, The calculation of small molecular interactions by the differences of separate total energies. Some procedures with reduced errors, Mol. Phys. 19 (1970) 553–566.

[55] M. J. Frisch, G. W. Trucks, H. B. Schlegel, G. E. Scuseria,A. Robb, J. R. Cheeseman, G. Scalmani, V. Barone, B. Mennucci, G. A. Petersson, H. Nakatsuji, M. Caricato, X. Li,H. P. Hratchian, A. F. Izmaylov, J. Bloino, G. Zheng,J. L. Sonnenberg, M. Hada, M. Ehara, K. Toyota, R. Fukuda,J. Hasegawa, M. Ishida, T. Nakajima, Y. Honda, O. Kitao,H. Nakai, T. Vreven, J. Montgomery, J. E. Peralta, F. Ogliaro, M. Bearpark, J. J. Heyd, E. Brothers, K. N.Kudin,V. N. Staroverov, R. Kobayashi, J. Normand, K. Raghavachari,A. Rendell, J. C. Burant, S. S. Iyengar, J. Tomasi, M. Cossi, N. Rega, J. M. Millam, M. Klene, J. E. Knox, J. B. Cross,V. Bakken, C. Adamo,J. Jaramillo, R. Gomperts, R.E. Stratmann,O. Yazyev, A. J. Austin, R. Cammi,C. Pomelli, J. W. Ochterski, R. L. Martin, K. Morokuma, V. G. Zakrzewski, G. A. Voth, P. Salvador, J. J. Dannenberg,S. Dapprich, A. D. Daniels, O. Farkas, J. B. Foresman, J. V. Ortiz, J. Cioslowski, D. J. Fox, Gaussian 09, RevisionD.01, Inc, Wallingford, CT (2009).

[56] F.A. Bulat, A. Toro-Labbé, T. Brinck, J.S. Murray, P. Politzer, Quantitative analysis of molecular surfaces: Areas, volumes, electrostatic potentials and average local ionization energies, J. Mol. Model. 16 (2010) 1679–1691.

[57] T. A. Keith, AIMALL, version 13.05.06, TK Gristmill Software: Overland Park, KS, 2013.

[58] E.D. Glendening, J.K. Badenhoop, A.E. Reed, J.E. Carpenter, J.A. Bohmann, C. M. Morales, C.R. Landis, F. Weinhold, Theoretical Chemistry Institute, University of Wisconsin, Madison, 2013.

[59] T. Lu, F. Chen, Multiwfn: A multifunctional wavefunction analyzer, J. Comput. Chem. 33 (2012) 580–592.

[60] W. Humphrey, A. Dalke, K. Schulten, VMD: Visual molecular dynamics, J. Mol. Graph. 14 (1996) 33–38.

[61] J. Contreras-Garcia, E.R. Johnson, S. Keinan, C. Robin, P. Jean-Philip, D. N. Beratan, W.T. Yang, NCIPLOT: A program for plotting noncovalent interaction regions, J. Chem. Theory Comput. 7 (2011) 625–632.

[62] P.F. Su, H. Li, Energy decomposition analysis of covalent bonds and intermolecular interactions, J. Chem. Phys. 131 (2009), 014102.

[63] M.W. Schmidt, K.K. Baldridge, J.A. Boatz, S.T. Elbert, M.S. Gordon, J.H. Jensen, S. Koseki, N. Matsunaga, K.A. Nguyen, S. Su, T.L. Windus, M. Dupuis, A. John, J. A. Montogomery, General atomic and molecular electronic structure system, J. Comput. Chem. 14 (1993) 1347–1363.

[64] G. Mahmoudi, A. Masoudiasl, M.G. Babashkina, A. Frontera, T. Doert, J.M. White, E. Zangrando, F.I. Zubkov, D.A. Safin, On the importance of π-hole spodium bonding in tricoordinated Hg II complexes, Dalton Trans. 49 (2020) 17547–17551.

[65] R. Wysokiński, W. Zierkiewicz, M. Michalczyk, S. Scheiner, Anion···anion attraction in complexes of MCl_3^- (M=Zn, Cd, Hg) with CN^-, ChemPhysChem 21 (11) (2020) 1119–1125.

[66] T. Xia, D. Li, L.J. Cheng, Theoretical analysis of the spodium bonds in $HgCl_2$···L (L= ClR, SR_2, and PR_3) dimers, Chem. Phys. (539) (2020) 110978.

[67] M. Jabłoński, Study of beryllium, magnesium, and spodium bonds to carbenes and carbodiphosphoranes, Molecules 26 (2021) 2275.